Long-range interactions in ring-shaped particle aggregates

M.-K. Müller & S. Luding
DelftChemTech, Particle Technology, TU Delft, Delft, Netherlands

ABSTRACT: A new hierarchical cell algorithm in combination with multi-pole expansions of the long-range forces in a Molecular Dynamics environment is presented. The model, based on the linked cell algorithm, is applied to ring-shaped particle aggregates. For such systems the relevance of the interplay of both short-ranged and long-ranged interactions will be the topic. We will present the time evolution of astrophysical objects with dissipation and self-gravitation, like e.g. massive planetary rings or dust disks orbiting around central objects. Of special interest is the cluster and structure formation of such particle systems in the presence of dissipation and self-gravity.

1 INTRODUCTION

For discrete particle systems with long-range interaction potentials like electrically charged granular gases or astrophysical rings with self-gravity it is always a challenge to handle the $1/r$-potential correctly, as it is shown and discussed in several fundamental books and publications (Eastwood et al. 1980; Barnes & Hut 1986; Allen & Tildesley 1987; Greengard & Rokhlin 1987; Barnes 1990).
The inclusion of particles' mutual gravitational forces in simulating astrophysical rings was first presented for azimuthally complete systems (Lukkari & Salo 1984), involving partially elastic collisions and gravitational encounters for a small number N of particles. Other authors (Wisdom & Tremaine 1988) consider only the vertical component of self-gravitation in the equations of motion in order to approximate the situation in Saturn's rings. The general importance of inelastic (dissipative) collisions in granular systems is shown in (Luding & Herrmann 1999).
While the computational time expense of the conventional treatment of long-range interacting particles (where all particles interact with all others) scales with $O(N^2)$, the new method described in this paper, the hierarchical linked cell algorithm (HLC), will lead to more efficient modeling. After a description of molecular dynamics and an introduction to the HLC algorithm, some results are shown. We use the mean vertical thickness of the rings for comparing this model with the conventional approach and will investigate how do short-ranged inelastic collisions interplay with long-ranged gravitational forces.

2 MOLECULAR DYNAMICS

Discrete particle molecular dynamics (MD) in 3D is used for numerical simulations of azimuthally complete ring systems. Time is discretized and for each (constant) time-step the equations of motion are integrated. Particles are treated as soft spheres and during a collision between particles i and j, with radii a_i and a_j, a linear repulsive force and dissipation of kinetic energy in normal direction, $\boldsymbol{n}_{ij} = \boldsymbol{r}_{ij}/r_{ij} = (\boldsymbol{r}_i - \boldsymbol{r}_j)/|\boldsymbol{r}_i - \boldsymbol{r}_j|$, is considered (see the linear spring dashpot model described in (Luding 1998)). The loss of kinetic energy at each collision is expressed by the coefficient of normal restitution $r = v_{ij}^{\prime(n)}/v_{ij}^{(n)}$ that gives the ratio of the relative velocities $v_{ij} = |\boldsymbol{v}_{ij}| = |\boldsymbol{v}_i - \boldsymbol{v}_j|$ in normal direction after (primed) and before (unprimed) the collision. The long-ranged forces are split into the external volume force (each particle interacts with the central potential with mass m_c) and self-gravitational force (each particle interacts with all others). To summarize, during a time-step on one ring particle i always long-ranged forces are acting,

$$\boldsymbol{F}_i^{\text{volume}} = -G\frac{m_i m_c}{r_{ic}^2}\frac{\boldsymbol{r}_{ic}}{r_{ic}} \quad (1)$$

$$\boldsymbol{F}_i^{\text{self}} = -Km_i \sum_{j=1,j\neq i}^{N} m_j \frac{\boldsymbol{n}_{ij}}{r_{ij}^2}\,, \quad (2)$$

and, if $r_{ij} < a_i + a_j$, short-ranged contact forces as well

$$\boldsymbol{F}_i^{\text{coll}} = k(a_i + a_j - r_{ij})\boldsymbol{n}_{ij} - \gamma_n(\boldsymbol{v}_{ij}\cdot\boldsymbol{n}_{ij})\boldsymbol{n}_{ij}\,. \quad (3)$$

Here is $r_{ic} = |\boldsymbol{r}_{ic}| = |\boldsymbol{r}_i - \boldsymbol{r}_c|$ the distance of i from the central mass with $\boldsymbol{r}_c$ as its position vector, γ_n a measure for how much kinetic energy is dissipated at each collision and k the spring constant that defines the stiffness of a contact. $K = cG$ defines via c the strength of the self-gravitation of the ring particles, where G denotes the gravitational constant.

3 THE MODEL

Our algorithm for handling long-range interaction potentials is set up onto a linked cell structure that is a regular lattice into which the system is divided and the particles are sorted, see also (Allen & Tildesley 1987). This gives the advantage that neighbor particle search and the computation of long-range forces (in the neighborhood) can be done in a single (first) step.

3.1 *Linked Cell Algorithm (LC)*

In order to avoid the computational time expense of $O(N^2)$ for collision detection for short-range forces of all particles with all other particles, the system is divided into $l \times m \times n$ linked cells with differently large edges. Each cell then has 26 neighbor cells, as it can be seen in Fig. 1. If the smallest LC size is larger than the largest particle diameter it is sufficient that particles in a (linked) cell of interest (coi) are checked for collision with particles only in neighboring cells because it is impossible that they encounter particles that are much more distant. This reduces the time expense to $O(NM)$, where M is the typical number of particles within coi and its 26 adjacent cells. Even though LC is efficient for mono-disperse systems it is less efficient for strongly poly-disperse particles (Muth et al. 2004).

3.2 *The Hierarchical Linked Cell Algorithm (HLC)*

The HLC method is built up on the linked cell structure and can be explained as follows: let us pick out one coi which we also call a hierarchy 0 (H0) cell. This coi and (in 3D) its 26 directly neighboring linked cells are important for the linked cell neighborhood search (as shown in Fig. 1) and, in the HLC context, represent one cell in the H1 level. In the same spirit 27 H1 cells make up one cell of H2 level – and so on. Note, that the higher level cells are all based on the present coi. Let us now construct an inner cut-off sphere around our particle of interest (poi) somewhere in coi, see Fig. 2, whose radius R_{in} equals the smallest LC edge for reasons of symmetry. For long-range interactions, all particles inside this sphere are treated separately, but those outside (but still inside the H1 level), for each single adjacent linked cell, are grouped together to pseudo-particles. Their masses and centers of mass are obtained from the particles inside the H0 cells they are made of. Obviously, in the H1 level, we have to consider 27 pseudo-particles interacting with poi. All particles in H2 contribute to 26 more pseudo-particles which interact with poi but are more distant. We can proceed this approach until the highest hierarchy H_{max} level is reached, approaching a computational time expense of $O(N\log_3 N)$, if $l = m = n$. Particular attention requires the implementation of an outer cut-off sphere with radius R_{out} inside level H_{max}, see also Fig. 2, for symmetry reasons. This problem will be discussed elsewhere.

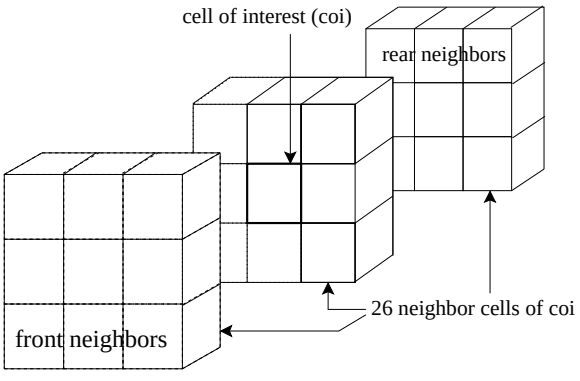

Figure 1. The three dimensional linked cell neighborhood, including the cell of interest (coi) and its 26 directly adjacent neighbor cells (front and rear cells are shifted apart from the other cells).

3.3 *Pseudo-particles and Multipole Expansion*

An ensemble of n_α particles can be composed into a pseudo-particle if the distances $r_{j\alpha}$ of the particles j of the ensemble α from the ensemble's center of mass

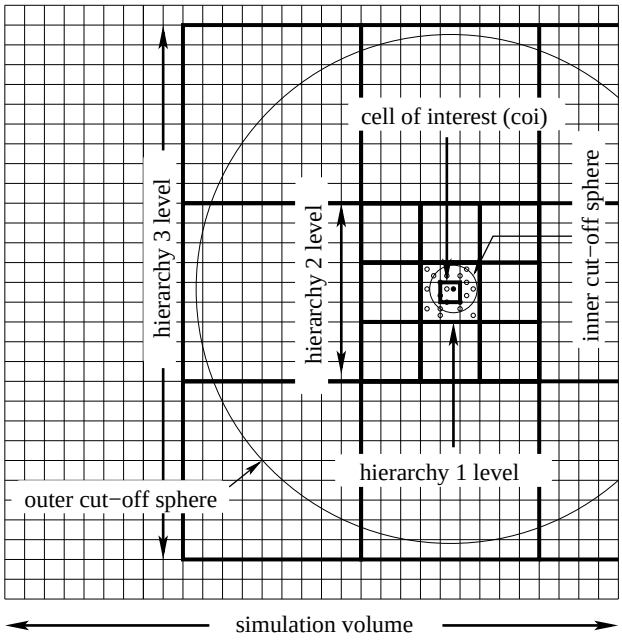

Figure 2. The HLC structure sets up onto the linked cell structure, shown in 2D for one linked cell as an example. Here is $H_{\text{max}} = 3$ with non-periodical boundaries.

are all much smaller than the distance $r_{i\alpha}$ of the *poi* from the center of mass of the ensemble. $R_{\rm in}$ mentioned in 3.2 represents a lower limit of $r_{i\alpha}$. A series expansion of the potential will then lead to monopole, dipole, quadrupole and higher terms in powers of the inverse distance $1/r_{i\alpha}$. The monopole term,

$$\boldsymbol{F}_{i\alpha}^{\rm self} = -K\frac{m_i\sum_{j=1}^{n_\alpha} m_j}{r_{i\alpha}^2}\frac{\boldsymbol{r}_{i\alpha}}{r_{i\alpha}}\,, \qquad (4)$$

looks similar to Eq. (2) but refers to only one distant pseudo-particle α. Dipole and quadrupole terms depend also on the ensemble of distances $r_{j\alpha}$ and can be found in several text-books.

4 RING-SHAPED PARTICLE AGGREGATES

In our simulations we distribute N = 9108 monodisperse particles of diameter $d = 2a$ = 0.000786 a.u. over a ring with mean radius R = 0.151 a.u. and an initial dynamical optical depth of τ = 0.3 (the ratio of the total surface area of particles to the area of the ring they reside in), which is actually a very dilute system. The following results are obtained during the first 0.3 Keplerian periods $T_{\rm Kep}$, where $T_{\rm Kep} \approx 415.000$ simulation time-steps. For a first investigation of the evolution of ring systems we implemented the HLC method only up to $H_{\rm max}$ = 2 and for the force calculation we use only the monopole term, see Eq. (4).
From various simulations of collisional dynamics of ring aggregates it is well-known (Pöschel & Luding 2001) that reaching a steady state depends drastically on the parameters of the dissipation model, i.e. on r. Each particle has, depending on its distance from the central potential, a certain azimuthal Keplerian velocity $v_{\rm Kep} = (Gm_c/r_{ic})^{1/2}$ which leads to differentially orbiting ring regions. The resulting shear stress transforms systematic into random motion, where the latter is equivalent to the temperature (standard deviation of particles' velocities) of the system and leads to a spreading of the ring. Dissipation counteracts this heating and gives rise to collisional cooling, governed by r. If r is chosen larger than a threshold value r_{cr} the ring will spread out both in radial and vertical direction, which is going ahead with an increasing temperature. If r lies below the threshold value the ring will be quasi-stable.

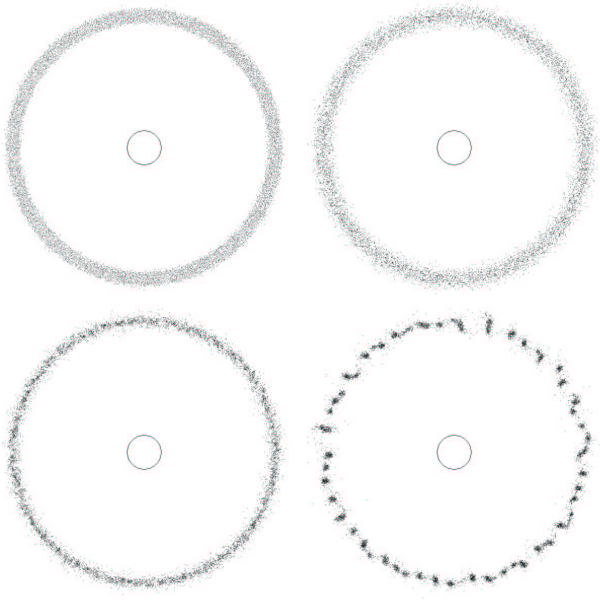

Figure 3. A ring aggregate of N = 9108 particles with no dissipation. Top left: initial configuration, t = 0. Top right: t = 0.3 $T_{\rm Kep}$, $c = 2\cdot 10^4$. Bottom left: t = 0.3 $T_{\rm Kep}$, $c = 2\cdot 10^5$. Bottom right: t = 0.3 $T_{\rm Kep}$, $c = 2\cdot 10^6$.

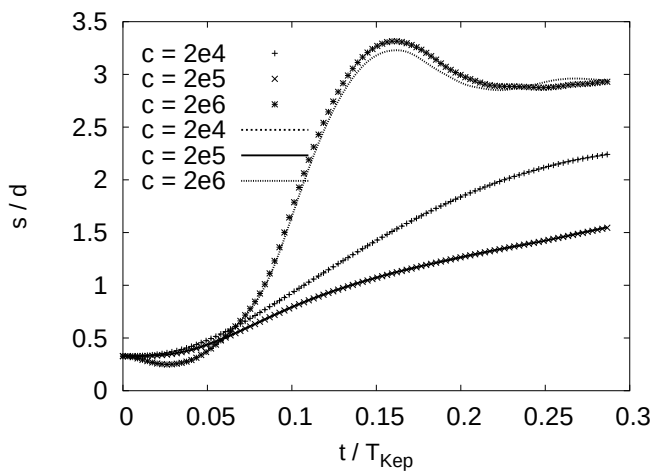

Figure 4. The scaled mean vertical height s/d is plotted against time in units of $T_{\rm Kep}$ for a qualitative comparison between the conventional approach (dots) and HLC algorithm (dashed lines), here is always r = 1.

Now, what is the effect of self-gravitation on the cooling process? Fig. 3 shows examples for non-dissipative (r = 1) simulations with different values of c. Quite remarkable is the early formation of lumps in the case $c = 2\cdot 10^6$. To evaluate the new method, in Fig. 4 the HLC implementation is compared with the N^2 method by observing the evolution of the mean vertical ring width s (twice the standard deviation of the vertical position components of all particles) in time. The results show only a little deviation from each other, even for the largest c value used. One can see here, that for stronger self-gravity the ring's relaxation time is much shorter than for weaker self-gravity.
In Fig. 5, a closer look to the interplay of self-gravity and dissipation is taken and again the time evolution of s is shown. In both panels the results with self-gravity are compared with those without, for different r. They show that for moderate mutual gravitational forces (top panel of Fig. 5) there is a weaker increase of height of the ring than it can be seen for the corresponding non-gravity results. This can be expected since the effects of gravitational attraction and granular cooling are acting against the effect of verti-

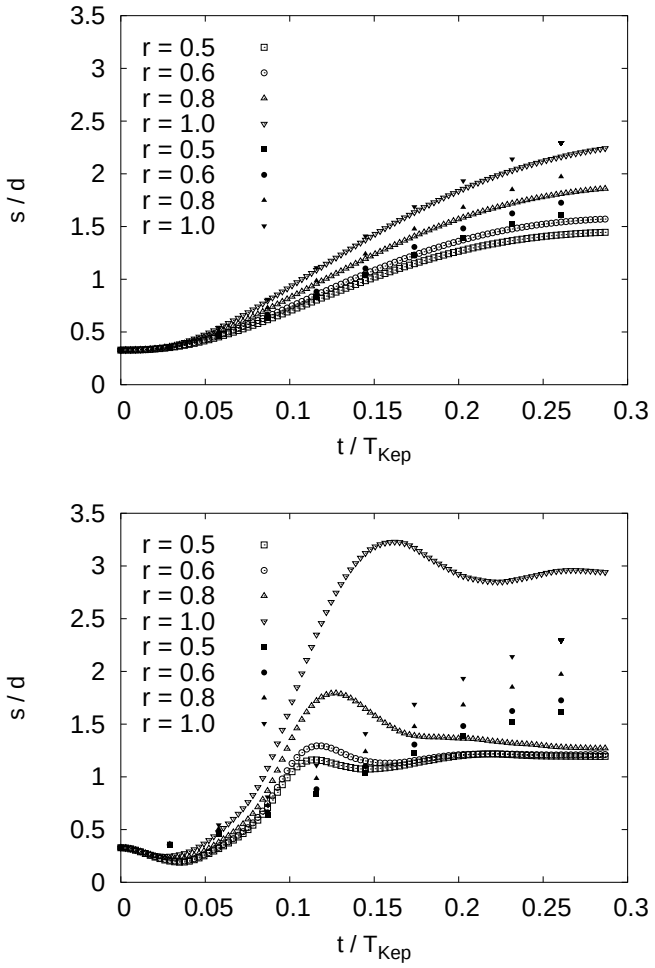

Figure 5. Scaled mean vertical height s/d plotted against time in units of $T_{\rm Kep}$. Top panel: comparison between self-gravity with $c = 2 \cdot 10^4$ (open symbols) and no self-gravity (solid symbols) for different dissipation r. Bottom panel: the same as in the top panel, but with $c = 2 \cdot 10^6$.

cal spreading. For stronger self-gravity (bottom panel of Fig. 5), in the beginning the self-gravitation contracts the ring stronger, but later on it causes s increasing faster than in the non-gravity case. After a strong increase, for all simulations (except for $r = 1$) s approaches the same saturation level, independent from r. In case of no dissipation, we observe a much stronger increase and no significant descent within the simulation time. Thus, with strong self-gravity, the elastic system behaves strongly different from the inelastic ones.

5 CONCLUSIONS

We introduced a new algorithm that allows for handling $1/r$-long-ranged potentials quite accurately. This method takes linked cells hierarchically up to larger length scales into account, shows nice agreement with the conventional N^2 approach and is faster. Only for strong forces there occur small differences between the curves. This can be the result of both the truncation of the long-range potential by the outer cut-off sphere already done in H2 level and the usage of only the monopole term in the force computation. Self-gravity generally tends to keep the ring narrow, i.e. the vertical height is smaller as compared to simulations with no self-gravity. Stronger self-gravity shows a shorter relaxation time, after which the ring has taken a steady-state. For high enough dissipation and strong self-gravity there can be observed a saturation level, which all the simulations have in common. In conclusion, we have shown that both dissipation and self-gravity affect the ring dynamics and thus must be taken into account.

ACKNOWLEDGEMENTS

This work is financially supported by the Delft Centre for Computational Science and Engineering (DCSE) of the Delft University of Technology.

REFERENCES

Allen, M. P. & Tildesley, D. J. 1987. *Computer Simulation of Liquids*. Oxford: Oxford University Press.

Barnes, J. 1990. A modified tree code. don't laugh; it runs. *J. of Comp. Phys.* 87: 161–170.

Barnes, J. & Hut, P. 1986. A hierarchical o(n log n) force calculation algorithm. *Nature* 324: 446–449.

Eastwood, J., Hockney, R., & Lawrence, D. 1980. P3m3dp - the 3-dimensional periodic particle-particle-particle-mesh program. *Comp. Phys. Commun.* 19: 215–261.

Greengard, L. & Rokhlin, V. 1987. A fast algorithm for particle simulations. *J. of Comp. Phys.* 73: 325–348.

Luding, S. 1998. Collisions & contacts between two particles. In H. J. Herrmann, J.-P. Hovi, & S. Luding (eds), *Physics of dry granular media - NATO ASI Series E350*: Dordrecht: 285. Kluwer Academic Publishers.

Luding, S. & Herrmann, H. J. 1999. Cluster growth in freely cooling granular media. *Chaos 9*(3): 673–681.

Lukkari, J. & Salo, H. 1984. Numerical simulations of collisions in self-gravitating systems. *Earth, Moon and Planets* 31: 1–13.

Muth, B., Müller, M.-K., Eberhard, P., & Luding, S. 2004. Contacts between many bodies. In W. Kurnik (ed.), *Machine Dynamics Problems*: Warsaw: 101–114.

Pöschel, T. & Luding, S. (eds) 2001. *Granular Gases*: Berlin. Springer. Lecture Notes in Physics 564.

Wisdom, J. & Tremaine, S. 1988. Local simulations of planetary rings. *Astron. J.* 95: 925–940.